

Alma Mater Studiorum Università di Bologna  
Archivio istituzionale della ricerca

Circuital Modeling of Polarization and Depolarization Currents in Polymeric Materials Under Low Electric Fields

This is the final peer-reviewed author's accepted manuscript (postprint) of the following publication:

*Published Version:*

Cambareri, P., de Falco, C., Di Rienzo, L., Seri, P., Montanari, G.C. (2023). Circuital Modeling of Polarization and Depolarization Currents in Polymeric Materials Under Low Electric Fields. IEEE TRANSACTIONS ON DIELECTRICS AND ELECTRICAL INSULATION, 30(3), 963-972 [10.1109/tdei.2023.3240974].

*Availability:*

This version is available at: <https://hdl.handle.net/11585/964488> since: 2024-02-29

*Published:*

DOI: <http://doi.org/10.1109/tdei.2023.3240974>

*Terms of use:*

Some rights reserved. The terms and conditions for the reuse of this version of the manuscript are specified in the publishing policy. For all terms of use and more information see the publisher's website.

This item was downloaded from IRIS Università di Bologna (<https://cris.unibo.it/>).  
When citing, please refer to the published version.

(Article begins on next page)

This is the final peer-reviewed accepted manuscript of:

**P. Cambareri, C. de Falco, L. Di Rienzo, P. Seri and G. C. Montanari, "Circuitual Modeling of Polarization and Depolarization Currents in Polymeric Materials Under Low Electric Fields," in *IEEE Transactions on Dielectrics and Electrical Insulation*, vol. 30, no. 3, pp. 963-972, June 2023**

The final published version is available online at:

<https://doi.org/10.1109/TDEI.2023.3240974>

Terms of use:

Some rights reserved. The terms and conditions for the reuse of this version of the manuscript are specified in the publishing policy. For all terms of use and more information see the publisher's website.

*This item was downloaded from IRIS Università di Bologna (<https://cris.unibo.it/>)*

***When citing, please refer to the published version.***

# Circuitual Modelling of Polarization and Depolarization Currents in Polymeric Materials under Low Electric Fields

P. Cambareri, C. de Falco, L. Di Rienzo, *Senior Member, IEEE*, P. Seri, *Member, IEEE* G. C. Montanari, *Fellow, IEEE*

**Abstract**— This paper proposes a circuitual model that describes polarization and depolarization currents observed in thin samples of polymeric materials under the application of an average electric field up to 30 kV/mm. The model employs the least possible number of parameters to fit the experimental measurements. A single carrier with negative charge is considered. The polarization curves are modelled by a power law to account for transport assisted by shallow traps. A model for the deep traps with a Gaussian distribution of the density of states is describes the depolarization curves. Experimental measurements made on various materials with different charging and discharging times suggest that a portion of the deep traps is filled within few seconds, while the time needed to release the trapped charges is in the order of several hours. The agreement between experimental and simulated currents confirms the validity of the proposed model, that can be seen as a generalization of the extended Debye model.

**Index Terms**—Insulation, polymers, electrostatics.

## I. INTRODUCTION

ELECTRIC systems are in the middle of a paradigm shift that is bringing them from a predominant AC operation to a hybrid AC/DC one, stimulated by the penetration of renewable energy sources and electrified mobility. In this situation, polymeric insulation may suffer intrinsic and/or extrinsic aging phenomena that must be known and accounted for at the design stage, for the sake of insulation system reliability [1]. Circuitual models can help to predict the stress levels causing such phenomena and their phenomenology. For example, they are used to calculate the partial discharge inception voltage in insulation, under AC or DC, which is fundamental to rule out extrinsic accelerated aging mechanism that can drastically reduce electrical apparatus reliability [2, 3]. Another example is provided by one of the basic diagnostic tests assessing quality and reliability of insulation systems, i.e., the polarization index, from which it is possible to relate variations of polarization properties to

aging and other types of phenomena [4]. Here, circuitual models can help in the interpretation of the experimental results, providing a conceptual framework to understand the causes of the changes in the dielectric properties.

In this paper, we focus on the aspect of polarization mechanisms in relation to conductivity measurements. The typical approach in the development of dielectric models, [5], is either to focus on microscopic processes and employ frameworks like the density functional theory to describe the mechanics of molecules and ions, or on macroscopic models that use Gauss law and drift-diffusion equations to describe the dynamics of charge carriers. This paper is ascribed to the category of macroscopic models.

Among macroscopic models, it is possible to develop various levels of sophistication. The physical phenomena are injection and extraction of carriers at the electrodes, trapping by shallow and deep traps, diffusion, and recombination. Injection is usually described by the Schottky law, even if there is some indication that it is not the most accurate model for dielectric/electrode interfaces [5]. The blocking effect of electrodes in extracting charge carriers has been studied mainly from a numerical point of view [7, 8]. Over time, various bipolar models involving electrons and holes as charge carriers were developed. In [9, 10] the injection through a Schottky barrier, constant mobility for shallow traps, single energy level for deep traps and recombination were considered, while neglecting diffusion. The work in [11] used similar hypotheses, but the authors introduced two additional species, namely positive and negative ions, and brought the diffusion mechanism into the equations. In [12] a model similar to [9, 10] was developed, but with field- and temperature-dependent mobility, non-linear conductivity based on the sinh law and diffusion of charge carriers. A comparison between models in older papers [9, 10] and those in more recent ones [11, 12] highlights an increasing level of sophistication, brought about by enhanced computing facilities. More complex models contain, in general, additional parameters that are estimated

P. Cambareri and L. Di Rienzo are with the Dipartimento di Elettronica, Informazione e Bioingegneria, Politecnico di Milano, 20133 Milano, Italy. C. de Falco is with the MOX, Dipartimento di Matematica, Politecnico di Milano, 20133 Milano, Italy. P. Seri is with the Laboratory of Innovative Materials for Electrical Systems (LIMES), Dipartimento di Ingegneria dell'Energia Elettrica e dell'Informazione, Università di

Bologna, 40136 Bologna, Italy. G. C. Montanari is with the Center for Advanced Power Systems, Florida State University, Tallahassee, FL 32306, USA.

Color versions of one or more of the figures in this article are available online at <http://ieeexplore.ieee.org>

either empirically, or from a mix of experimental and literature data that may require non-trivial fitting techniques [13].

This paper proposes an alternative approach, by developing a macroscopic circuit model that employs the least possible number of parameters. This is a step forward relative to the authors' previous work [14]. The rationale behind this approach is the focus on measurements of polarization and depolarization currents (PDC) to estimate the parameters: the information attainable from the PDC measurements is limited, and a model aiming to describe them should reflect this limitation without introducing misleading details [15].

The model assumes a continuous distribution of the density of states (DOS) for the deep traps. Experiments based on surface potential decay and thermally stimulated depolarization currents suggest that the trap distribution is a superposition of Gaussian distributions [6, 16]. In the view of simplifying the approach the DOS is a single Gaussian.

The applied electric field is supposed to be relatively low compared to other works. The samples were tested at 10 kV/mm and 30 kV/mm. Under moderate field values, which, however, are very close to those used for DC cable design, injection, extraction, and recombination processes may not play a central role. Charge dynamic seems to be dominated by trapping and detrapping [10]. As a first approximation recombination is neglected. Under low fields and negligible recombination there is some evidence, especially in polyethylene-based polymers, that the net trapped charge is unipolar [9, 17]. The model assumes then a single carrier species with negative charge.

The model neglects the diffusion of carriers, which is a common assumption [5, 9, 10]. The transport through the bulk is attributed to the drift current. Shallow traps are involved in the drift mechanism by exchanging carriers with the conduction and valence bands, and tunnelling (hopping mechanism) [5, 6]. Injection provides most of the charge carriers involved in these processes. To simplify the approach, we consider infinite charge availability for transport rather than introducing a specific law for injection and extraction of carriers.

As it will be shown in section 3, deep traps immediately capture the carriers as voltage is turned on, but the release after voltage removal is much slower. This means that polarization is mostly controlled by the drift current, which is given by carrier hopping in shallow traps and modelled by a power law [18, 19]. On the contrary, the dynamic of deep traps dominates during depolarization, and it is modelled using the theory by Simmons and Tam [20]. In the model proposed here deep and shallow traps do not exchange carriers with each other, giving origin to two independent dynamics.

The behavior of polymers under medium-high electric fields is affected by space charge, which increases the risk of short-term dielectric breakdown [21] and causes accelerated aging over time [22]. The proposed model does not predict the space charge dynamic. It estimates what can be addressed as the "ideal behavior" of the material., and space charge is treated as a disturbance. From a practical point of view this is not necessarily a limitation. The development of polymeric insulation technology seeks solutions to suppress space charge,

bringing the material response closer to the ideal behavior. For example, in [23] it is shown how deep traps introduced in polypropylene by grafting styrene functional groups on the molecular chains suppress space charge accumulation.

This introduction has, hopefully, provided the proper context for the proposed model, which differs substantially from the typical macroscopic models presented in the literature. In sections 2 and 3 we will describe the experimental setup and the mathematical model. Validation, reported in sections 4 and 5, is based on four different materials: three polypropylene-based polymers and one sample of XLPE. Finally, section 6 will discuss the impact of space charge on the ideal behavior.

## II. MEASUREMENT SETUP AND SAMPLES

PDC were measured with a custom setup that includes a DC voltage source, an electrometer, and a conductivity cell built in-house. The samples were thermally pre-treated and had gold-sputtered electrodes with a diameter of 26 mm and a guard ring. The system has a resolution of 0.001 pA, with a background noise of 0.1 pA. More details on the setup are given in [24].

The DC voltage source applied during polarization had an intrinsic transient that is represented by

$$v_s(t) = V[1 - \exp(-t/\tau_g)], \quad (1)$$

where  $\tau_g$  is 2.5 s. Likewise, an exponential transient occurs during depolarization, when voltage is turned off. The time constant is approximately the same as in polarization. The generator transient, then, is

$$v_s(t) = V \exp(-t/\tau_g). \quad (2)$$

The tested objects were three different samples of polypropylene (PP) and one sample of XLPE. The shape of the samples was cylindrical, with a base area of 5.31 cm<sup>2</sup>. Table I summarizes their characteristics. PP1 underwent a sequence of five polarization and depolarization cycles. The polarization time was increased from 10 s to 10<sup>5</sup> s, while the depolarization time was fixed at 10<sup>5</sup> s. PP2 underwent a sequence of four polarization and depolarization cycles, plus one final polarization. The polarization time was 10<sup>5</sup> s (except for the last one that was 10<sup>4</sup> s), the depolarization time decreased from 10<sup>5</sup> s to 5 s. PP3 and XLPE underwent one cycle of polarization and depolarization transients at different temperatures and fixed electric field. Each sample was pre-treated before each new polarization. The polarization time was 10<sup>5</sup> s, the depolarization time was between 10<sup>3</sup> s and 10<sup>4</sup> s.

TABLE I

TEST CONDITIONS OF THE SAMPLES

Sample	Field	Temperature	Thickness
PP1	10 kV/mm	60 °C	0.5 mm
PP2	30 kV/mm	60 °C	0.5 mm
PP3	30 kV/mm	30 °C, 60 °C, 90 °C	0.35 mm
XLPE	30 kV/mm	20 °C, 60 °C, 90 °C	0.2 mm

### III. MODEL

When voltage is applied to the sample shallow and deep traps capture the injected charges. The former are typically physical traps, the latter may have a chemical origin. Deep traps can quickly capture the carriers [25]. The three fundamental processes in the model are transport assisted by shallow traps (drift current), trapping and detrapping by deep traps, and polarization processes. The measured current, during both polarization and depolarization, can be written as

$$i_m = Gv_s + \dot{B} + C\dot{v}_s + i_{sp}. \quad (3)$$

The first term,  $Gv_s$ , is the drift current and  $G$  is a time-dependent conductance.  $\dot{B}$  is the current from the deep traps, which is positive when the charges are captured and negative when they are released. Thus,  $B$  is the trapped charge. The third term,  $C\dot{v}_s$ , is the current of the fast polarization processes [14, 18], namely atomic and ionic polarization, and  $C$  is a capacitance proportional to the relative permittivity of the material,  $\epsilon_r$ . The last term,  $i_{sp}$ , is the current due to the slow polarization processes [14, 18], typically dipolar and interfacial polarization, that are modeled as a Debye relaxation process [18, 26]. Dipolar and interfacial polarizations take place in the polymeric chains of the dielectric and at the interfaces, that are present in the insulation system either by design, as for a mixed insulation, or due to external sources, like water trees [27].

Equation (3) corresponds to the circuit of Fig. 1. In each branch of the circuit flows one component of  $i_m$ . There may be more than one R-C branches associated to  $i_{sp}$ , depending on the number of slow polarization processes identified from the measurements. The branch with two parallel controlled current sources in series with capacitor  $S_B$  models the deep traps. It is described in detail in the next subsection. The circuit in Fig. 1 is a generalization of the extended Debye model [18, 26].

Each term of equation (3) is significant in different parts of the polarization and depolarization transients. The drift current,  $Gv_s$ , may predominate for long polarization times, as the deep traps are almost full and  $\dot{B}$  is negligible. During depolarization  $\dot{B}$  plays the major role, as the deep traps release the captured carriers. The polarization processes,  $C\dot{v}_s$  and  $i_{sp}$ , take place for both short and long times, even if in the long-term they may be overwhelmed by trapping and detrapping [24].

#### A. Deep traps

The model considers a Gaussian distribution for the DOS:

$$g(E) = \frac{N}{\alpha\sqrt{2\pi}} \exp\left[-\frac{(E+\Delta E)^2}{2\alpha^2}\right], \quad (4)$$

where  $N$ , measured in  $C/m^3$ , is the total charge that can be trapped per unit volume,  $\Delta E$  and  $\alpha$ , measured in joule, are the mean trap depth and the trap distribution width. Assuming that deepest traps are filled first, the trapped charge density is a function of the highest occupied level,  $E_{\max}$ :

$$b = \int_{-\infty}^{E_{\max}} g(E) dE = F(E_{\max}). \quad (5)$$

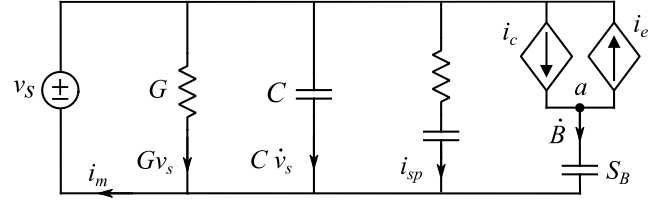


Fig. 1. Circuit model of the polymer.

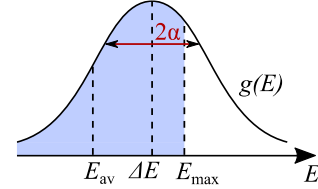


Fig. 2. The DOS with its parameters  $\Delta E$  and  $\alpha$ , and the maximum and average energies.

It is better to write  $b$  in terms of the average occupation energy,

$$E_{av} = \frac{\int_{-\infty}^{E_{\max}} E g(E) dE}{\int_{-\infty}^{E_{\max}} g(E) dE} = -\Delta E + \sqrt{\frac{2\alpha^2}{\pi}} \frac{e^{-\frac{(E_{\max}+\Delta E)^2}{2\alpha^2}}}{\text{erfc}\left(\frac{E_{\max}+\Delta E}{\sqrt{2}\alpha}\right)-2}} \quad (6)$$

and let  $E_{av} = \Gamma(E_{\max})$ . Fig. 2 depicts the features of the DOS.

Function  $g(E)$  is strictly positive, so  $F(E_{\max})$  is monotonic and invertible. Therefore,

$$E_{\max} = F^{-1}(b) = -\Delta E + \sqrt{2} \alpha \text{erf}^{-1}\left(\frac{2b}{N} - 1\right) \quad (7)$$

where  $\text{erf}^{-1}$  is the inverse error function. Using (6) and (7), we can then write the relation between  $E_{av}$  and  $b$ :

$$E_{av} = \Gamma(F^{-1}(b)). \quad (8)$$

The rate at which the charges are captured by the deep traps depends on the number of unoccupied trap states and on the trap capture cross-section,  $c_s$ , that is measured in  $m^2$ :

$$\dot{b}_c = c_s j_d \frac{N-b}{e}, \quad (9)$$

where  $j_d$  is the drift current density, and  $e$  is the quantum of charge. The rate at which the carriers escape depends on the energy of the occupied trap states [17]. Using the average occupation energy,  $E_{av}$ , the escape rate is given by

$$\dot{b}_e = \nu_0 b \exp\left(\frac{E_{av}+\Delta E}{k_B T}\right), \quad (10)$$

where  $\nu_0$  is the attempt-to-escape rate when the DOS is completely filled,  $k_B$  is the Boltzmann constant and  $T$  is the temperature. The net trapping current,  $\dot{b}$ , is given by the balance between the capture and escape currents:

$$\dot{b} = \dot{b}_c - \dot{b}_e = c_s j_d \frac{N-b}{e} - \nu_0 b \exp\left(\frac{E_{av}+\Delta E}{k_B T}\right). \quad (11)$$

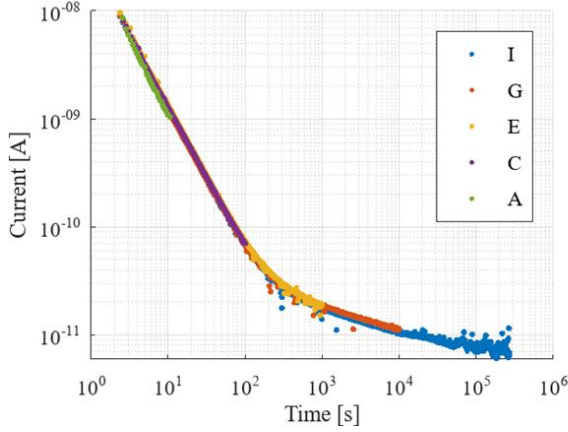


**Fig. 3.** Polarization currents measured in PP1. The duration of the transient increases in each cycle: current A is the shortest (10 s), current I is the longest ( $2.7 \cdot 10^5$  s).

To match equation (11) with (3) the average trapped charge is defined as  $B = A \cdot d \cdot b$ , being  $A$  the sample's area and  $d$  the thickness. Then, equation (11) multiplied by  $A \cdot d$  and the following quantities are defined:

$$\tilde{N} = N \cdot A \cdot d, \quad (12)$$

$$S = \frac{c_s}{eA}, \quad (13)$$

$$i_c = \dot{b}_c \cdot A \cdot d = S \cdot G v_s \cdot (\tilde{N} - B), \quad (14)$$

$$i_e = \dot{b}_e \cdot A \cdot d = v_0 B \exp\left(\frac{E_{av} + \Delta E}{k_B T}\right), \quad (15)$$

In (14) the term  $j_d A$ , which is the drift current, was replaced by  $G v_s$ , that appears in (3). In this way,  $\dot{B} = i_c - i_e$ , thus

$$\dot{B} = S G v_s (\tilde{N} - B) - v_0 B \exp\left(\frac{E_{av} + \Delta E}{k_B T}\right). \quad (16)$$

Equation (16) models the trapping branch of the circuit in Fig. 1: it is the Kirchhoff current law at node  $a$ . The origin of capacitor  $S_B$  can be understood by defining the quantity

$$\tau(B) = \tau_0 \exp\left(-\frac{E_{av} + \Delta E}{k_B T}\right), \quad (17)$$

where  $\tau_0 = v_0^{-1}$ . With this definition  $i_e = B/\tau(B)$  and equation (16) becomes

$$\dot{B} + \frac{B}{\tau(B)} = i_c, \quad (18)$$

or, equivalently, with  $1/\tau(B) = G_B S_B(B)$ ,

$$\dot{B} + G_B S_B(B) B = i_c, \quad (19)$$

where  $G_B$  is a conductance and  $S_B(B)$  is a charge-dependent elastance representing the non-linear capacitor in Fig. 1.

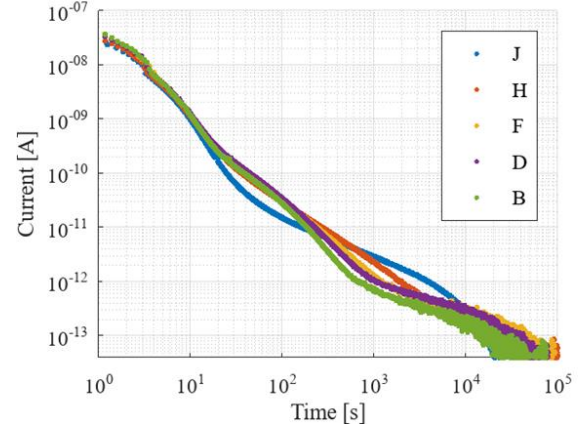


**Fig. 4.** Depolarization currents measured in PP1. Currents B, D, F and H are mostly overlapping, except for the interval between  $2 \cdot 10^2$  s and  $3 \cdot 10^3$  s.

### B. Time-varying conductance

The drift current,  $G v_s$ , depends on conductance  $G$ , that is related to the conductivity of the material.  $G$  is modeled empirically from the experiments. Figs. 3 and 4 show the PDC in PP1. When the voltage is applied the first time, current A in Fig. 3 is measured. Then voltage is removed, and the electrometer measures current B in Fig. 4. When voltage is reapplied current C in Fig. 3 is observed, and so on for the remaining cycles. The polarization currents in Fig. 3 follow the same trend in each cycle. The curves resemble a power law approaching the steady state. Since after an initial transient the applied voltage is constant,  $v_s = V$ , the transient behavior of the drift current must be ascribed to a variation of the conductance:

$$G(t) = G_2 + (G_1 - G_2) \cdot (1 + t)^{-n}, \quad (20)$$

where  $G_1$  is the conductance at 0 s,  $G_2$  is the steady-state value and  $n$  is a free parameter. While the duration of the polarization currents in Fig. 3 increases from A to I, all the depolarization currents in Fig. 4 need  $10^5$  s to reach  $10^{-13}$  A, which is the accuracy limit of the measurement system. This suggests that the detrapping currents in Fig. 4 are not affected by the duration of the previous polarization, which confirms the idea that the deep traps are quickly populated as voltage is turned on.

In the testing procedure of PP2 the polarization was carried on until the steady state, while the duration of the depolarization was shortened after each cycle. The results are shown in Figs. 5 and 6, and their interpretation is analogous to Figs. 3 and 4. The depolarization currents in Fig. 6 follow the same trend in each cycle, but the same does not happen for the polarization currents in Fig. 5. Let us focus on the highlighted region in Fig. 5, which covers the time range between 20 s and 40 s, coinciding with the first stage in which the generator is at steady state ( $v_s = V$ ). Here, currents A and C are similar. Since the depolarization transient between them is relatively long ( $10^4$  s, current B in Fig. 6), a long depolarization transient does not seem to affect the subsequent polarization. If the depolarization transient duration is halved to  $5 \cdot 10^3$  s, as for current D in Fig. 6, the matter is different. Looking at the sequence C – D – E it is

evident that halving the depolarization transient causes a reduction of current  $E$  with respect to  $C$ , in the highlighted region. This suggests that shorter depolarizations have an impact on the subsequent polarizations. The same argument applies to the sequence  $E - F - G$ , in which the depolarization current  $F$  lasts only 50 s. An extreme case is current  $H$  in Fig. 6, since its transient holds only for 5 s: here the difference between the previous and the subsequent polarizations, i.e., currents  $G$  and  $I$  in Fig. 5, is negligible.

The polarization current under constant voltage is attributed to the drift current,  $G(t)V$ , so the previous discussion implies that the depolarization transient duration affects  $G(t)$ . During polarization the conductance falls from the initial value  $G_1$  to the steady-state value  $G_2$ . During depolarization a restoring process brings  $G(t)$  back to the initial value  $G_1$ . Fig. 7 summarizes this behavior. An exponential with time constant  $\tau_a$  describes the restoring process.  $G$  becomes, in general,

$$G(t) = a(t) G_1 + (1 - a(t)) G_2, \quad (21)$$

and  $a(t)$  is governed by the following equations:

$$\dot{a} = \begin{cases} -n a^{\frac{n+1}{n}} & v_s \geq V_{tr} \\ -\frac{1}{\tau_a} (a - 1) & v_s < V_{tr} \end{cases}. \quad (22)$$

$V_{tr}$  is an empirical threshold voltage and the initial condition is  $a(0) = 1$ . The first equation in (22) models the power law (20), the second equation models the conductance-restoring process.

#### IV. FITTING OF MEASUREMENTS WITH VARIABLE CHARGING AND DISCHARGING TIME

The parameters that fit the polarization currents, as shown by (21) and (22), are:  $G_1$ ,  $G_2$ ,  $n$ ,  $\tau_a$  and  $V_{tr}$ . From (11) and the preceding equations, the fitting parameters of the depolarization currents are  $N$ ,  $\alpha$ ,  $\Delta E$ ,  $v_0$  and  $c_s$ . Moreover, the relative permittivity,  $\epsilon_r$ , is necessary to determine  $C = \epsilon_0 \epsilon_r A/d$  in (3). This yields 11 fitting parameters, however, let us consider the exponential term in equation (11),  $\exp[(E_{av} + \Delta E)/(k_B T)]$ . Using (5), (6), (7) and (8), this term becomes

$$\exp \left\{ -\sqrt{\frac{2}{\pi}} \cdot \frac{\alpha}{k_B T} \cdot \frac{N}{2b} \cdot e^{-\left[ \text{erf}^{-1} \left( \frac{2b}{N} - 1 \right) \right]^2} \right\}. \quad (23)$$

The trap distribution center,  $\Delta E$ , is not present in (23), thanks to an algebraic simplification, thus it is not a fitting parameter. Based on the experience built on fitting the PDC curves, the authors also realized that  $v_0$  and  $c_s$  do not change between different materials and that it is sufficient to provide an adequate order of magnitude for them:  $v_0$  was fixed to  $10^{12} \text{ s}^{-1}$  [11, 12, 25];  $c_s$  was empirically estimated and fixed to  $10^{-14} \text{ m}^2$ . Therefore, the depolarization curves are fitted only with  $N$  and  $\alpha$ . The same argument can be proposed on  $V_{tr}$ , that was fixed at 100 V. The minimum number of parameters required to fit to a PDC measurement is ultimately reduced to 7.

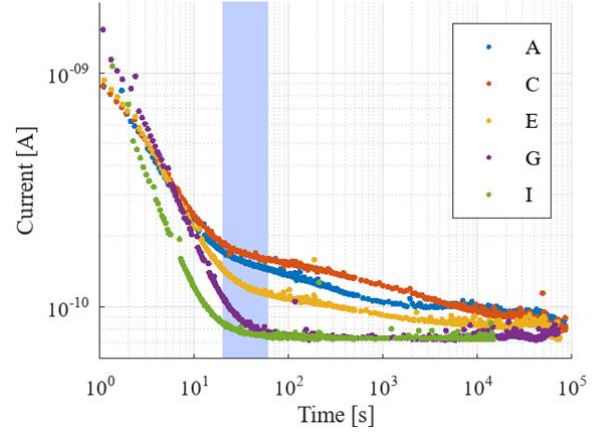


Fig. 5. Polarization currents measured in PP2. The transient is carried on until  $10^5$  s. The highlighted vertical band covers the time range between 20 s and 40 s.

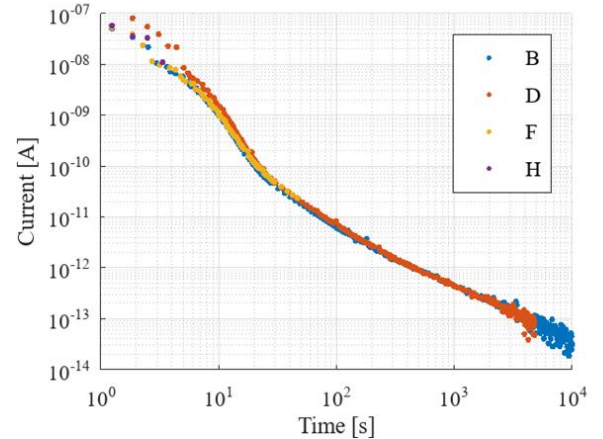


Fig. 6. Depolarization currents measured in PP2. The transient duration is shortened after each cycle.

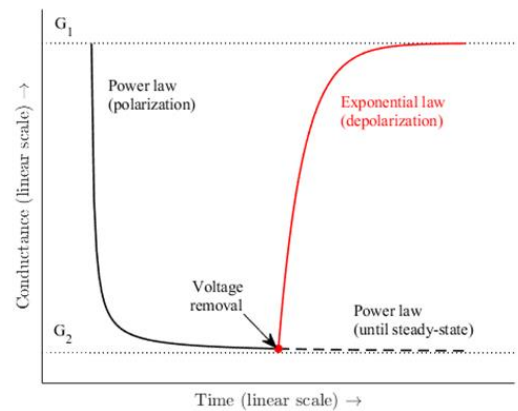


Fig. 7. Time-varying conductance. During polarization  $G(t)$  is a power law (solid, black line). If the polarization is sufficiently long,  $G(t)$  reaches the steady-state value,  $G_2$  (dashed, black line). If voltage is removed and the depolarization transient begins, the conductance rises to the initial value  $G_1$ , following an exponential law (red line).

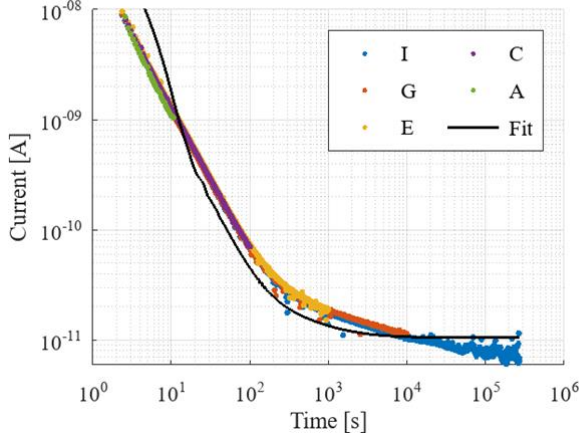


Fig. 8. Fitting of polarization currents in PP1.

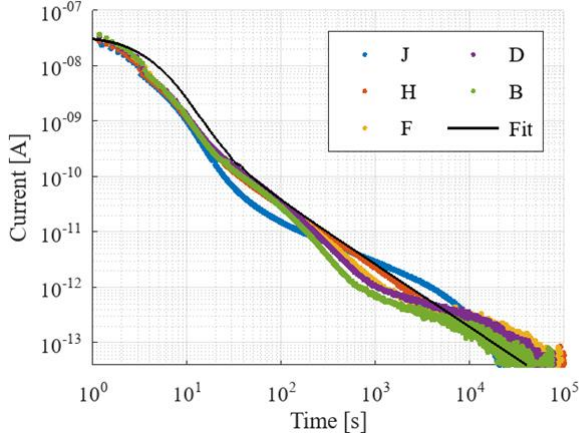


Fig. 9. Fitting of depolarization currents in PP1.

Figs. 8 and 9 show the fitting of the PDC in PP1. In both figures only one fitting curve is shown, since the behavior of both the polarization and depolarization currents obtained from the model follows the same trend in each cycle.

Figs. 10 and 11 show the fitting of the PDC in PP2. In Fig. 9 the fitting is quite accurate after 20 s, which means that the behavior of  $G(t)$  has been reconstructed correctly. In the first 20 s the fitting is not accurate, but this matter will be discussed in section 6. In Fig. 11 only the longest depolarization is shown because all the currents have the same trend in each cycle.

Table 2 reports the fitting parameters for PP1 and PP2. PP2 was the only sample with the appropriate PDC measurements to fit the value of  $\tau_a$ .

TABLE II

MODEL PARAMETER ESTIMATES FROM POLARIZATION AND DEPOLARIZATION CURRENT CURVES FOR PP1 AND PP2.

Parameter	PP1	PP2
$\epsilon_r$	2.6	2.6
$G_1$ [S]	$7.4 \cdot 10^{-12}$	$2.5 \cdot 10^{-14}$
$G_2$ [S]	$2.1 \cdot 10^{-15}$	$4.9 \cdot 10^{-15}$
$n$	1.3	0.3
$\tau_a$ [s]	-	$6.0 \cdot 10^3$
$N$ [C/m <sup>3</sup> ]	1.7	0.1
$\alpha$ [eV]	0.5	0.75

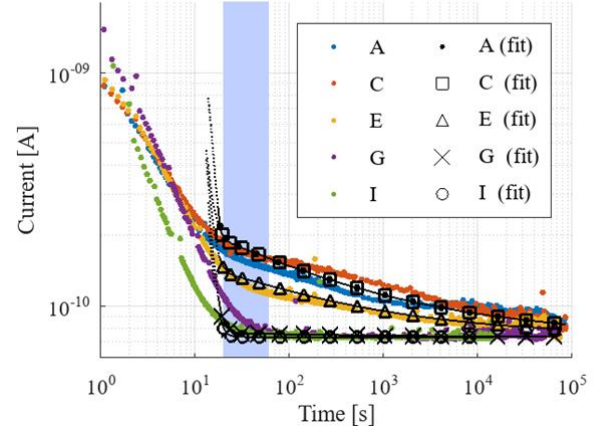


Fig. 10. Fitting of polarization currents in PP2. Currents A (fit) and C (fit) are overlapped, as well as currents G (fit) and I (fit). The highlighted vertical band covers the time range between 20 s and 40 s.

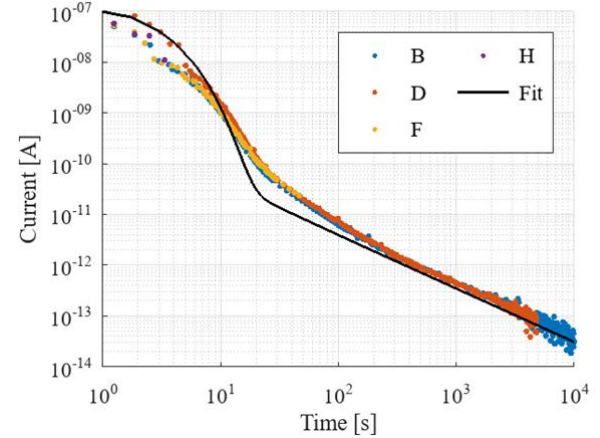


Fig. 11. Fitting of depolarization currents in PP2.

## V. FITTING OF MEASUREMENTS AT DIFFERENT TEMPERATURES

When materials are tested at different temperatures some of their properties change. Therefore, some of the model parameters are expected to change as well with temperature. This section focuses on PP3 and XLPE, that were tested at three different temperatures (see Table 1).

Table 3 reports the fitting parameters of PP3 for each temperature. The ones exhibiting a significant temperature dependence are  $G_1$ ,  $G_2$  and  $n$ , i.e., those associated with the shallow traps. There may be a temperature dependence also for  $\tau_a$ , but the lack of suitable experiments for PP3 prevented the retrieval of this information. The fitting of the polarization curves is reported in Fig. 12. It shows that the result is acceptable after approximately 20 s at all temperatures. There is a deviation between the experiment and the fitting occurring between  $5 \cdot 10^3$  s and  $2 \cdot 10^4$  s at 30 °C, and a similar one occurs at 90 °C, between  $2 \cdot 10^2$  s and  $4 \cdot 10^4$  s. The deviations between fittings and experiments are discussed in section 6.

TABLE III

MODEL PARAMETER ESTIMATES FROM POLARIZATION AND DEPOLARIZATION CURRENT CURVES FOR PP3.

Parameter	30°C	60°C	90°C
$\epsilon_r$	2.6	2.6	2.6
$G_1$ [S]	$4.0 \cdot 10^{-13}$	$2.4 \cdot 10^{-13}$	$1.6 \cdot 10^{-12}$
$G_2$ [S]	$2.0 \cdot 10^{-16}$	$1.8 \cdot 10^{-14}$	$1.4 \cdot 10^{-13}$
$n$	1.1	0.4	0.3
$N$ [C/m <sup>3</sup> ]	0.1	0.1	0.1
$\alpha$ [eV]	0.75	0.75	0.75

The relative permittivity,  $\epsilon_r$ , is temperature-independent, at least in the operating temperature range of an insulating material [18]. The authors found that  $N$  and  $\alpha$ , the parameters of the deep traps, provided an acceptable fitting without changing with temperature. Fig. 13 shows the fitting of the depolarization curves. All the fitting currents are very close to each other: this is an indication that temperature does not have a significant impact in the model. The fitting seems acceptable for currents at 90 °C and 60 °C. The spike occurring at  $2 \cdot 10^3$  s in the current at 60 °C was likely due to a disturbance during the measurement. The fitting at 30 °C is acceptable after  $10^3$  s.

The simulated currents help to identify the dominant components in equation (3) in each part of the transient. As a reference, Figs. 14 and 15 show the components of the PDC measured in PP3 at 60 °C. In Fig. 14, the first 20 s are dominated by the current associated with fast polarization processes,  $C\dot{v}_s$ . After 20 s, the detrapping current,  $\dot{B}$ , rules the discharge, meaning that we observe the charges released by the deep traps. In Fig. 15, the first 20 s of the simulated current are still dominated by  $C\dot{v}_s$ , even if the model is not supported by the experimental data. For longer times the drift current,  $Gv_s$ , prevails and the agreement with the experiment is good.

The initial polarization current,  $C\dot{v}_s$ , is the same in both Figs. 14 and 15. This is not evident from the pictures because of the different axis scales. This current is due to the capacitive branch of the circuit in Fig. 1, which behaves symmetrically in both polarization and depolarization because we assumed that the time constant of the generator,  $\tau_g$ , was constant.

Table 4 resumes the fitting parameters of the XLPE sample. Two additional parameters have been introduced with respect to PP3,  $R_{sp}$  and  $C_{sp}$ , that are those of the RC branch in Fig. 1.

TABLE IV

MODEL PARAMETER ESTIMATES FROM POLARIZATION AND DEPOLARIZATION CURRENT CURVES FOR XLPE.

Parameter	20°C	60°C	90°C
$\epsilon_r$	2.3	2.3	2.3
$R_{sp}$ [ $\Omega$ ]	$4.4 \cdot 10^{11}$	$4.4 \cdot 10^{11}$	$4.4 \cdot 10^{11}$
$C_{sp}$ [F]	$8.0 \cdot 10^{-12}$	$8.0 \cdot 10^{-12}$	$8.0 \cdot 10^{-12}$
$G_1$ [S]	$1.0 \cdot 10^{-13}$	$1.2 \cdot 10^{-13}$	$1.6 \cdot 10^{-14}$
$G_2$ [S]	$3.0 \cdot 10^{-17}$	$1.6 \cdot 10^{-15}$	$1.6 \cdot 10^{-14}$
$n$	0.9	0.6	0.5
$N$ [C m <sup>-3</sup> ]	0.3	0.3	0.3
$\alpha$ [eV]	0.5	0.5	0.5

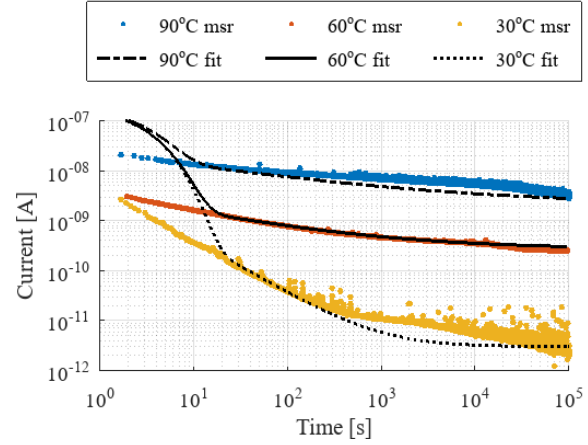


Fig. 12. Fitting of polarization currents in PP3 at different temperatures.

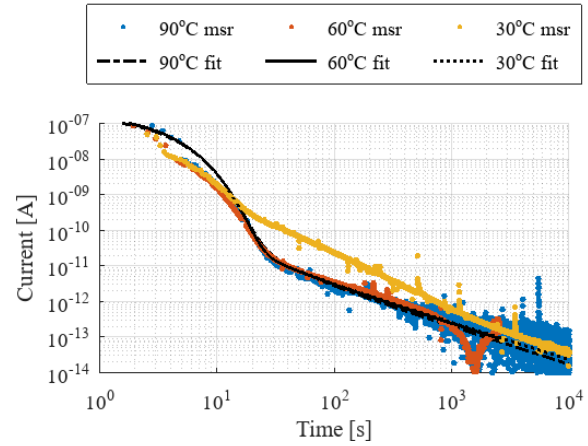


Fig. 13. Fitting of depolarization current measurements in PP3 at different temperatures. The fitting curves overlap with each other.

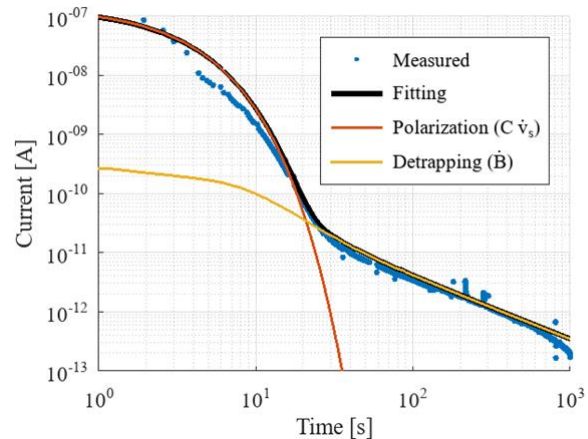


Fig. 14. Depolarization components, PP3 at 60 °C.

This branch was necessary because current  $C\dot{v}_s$  was not sufficient to accurately reproduce the first 20 s of the depolarization transients, as illustrated by Fig. 16.

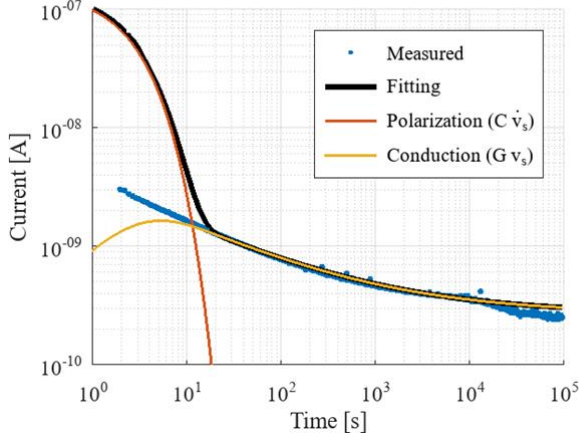


Fig. 15. Polarization components, PP3 at 60 °C.

Figs. 17 and 18 show the fitting of the PDC in XLPE. In Fig. 17 the fitting is not particularly accurate within the first 20 s. For times longer than 20 s the measured current at 20 °C exhibits an oscillation compared to the corresponding fitting: the experimental current lies below the fitted one between 30 s and  $5 \cdot 10^3$  s and above between  $5 \cdot 10^3$  s and  $10^4$  s. At 60 °C and at 90 °C the experimental current lies below the fitted one between 40 s and  $6 \cdot 10^3$  s.

In Fig. 18 the fitting is very good at all temperatures in the first 20 s of the transient. Beyond the first 20 s different deviations from the experiments occur. At 20 °C the fitting is good between 20 s and 200 s, then the experimental current deviates slightly above the fitting one. At 60 °C the experimental current lies above the fitting one between 20 s and 100 s, then the two curves reconcile with each other and are in good agreement. The fitted current at 90 °C is overlapped to the one at 60 °C. In this case the deviation between model and experiment is enhanced, being the measured current above the fitted one between 20 s and  $10^3$  s.

Overall, the presented results show that the model, within some limitations, provides an acceptable fitting of the experimental results. Deviations between model and experiments are discussed in the next section.

## VI. DISCUSSION

The presence of space charge in the samples may cause the discrepancy observed between the fitting currents and the measured ones. To verify this idea, we estimate the charge related to the deviation between experiments and model as

$$\rho_s(t) = \frac{1}{A \cdot d} \int_{t_0}^t |i_{\text{msr}}(t) - i_{\text{fit}}(t)| dt, \quad (24)$$

where  $i_{\text{msr}}$  is one of the currents measured during the PDC tests and  $i_{\text{fit}}$  is the corresponding fitting;  $t_0$  is the time at which the first current measurement occurs, and it is greater than 0 s. To support the idea that space charge can be involved in the misfitting, pulsed electroacoustic (PEA) measurements, [28], were performed on similar specimens to those used for Figs. 12, 13, 17 and 18, namely PP3 and XLPE.

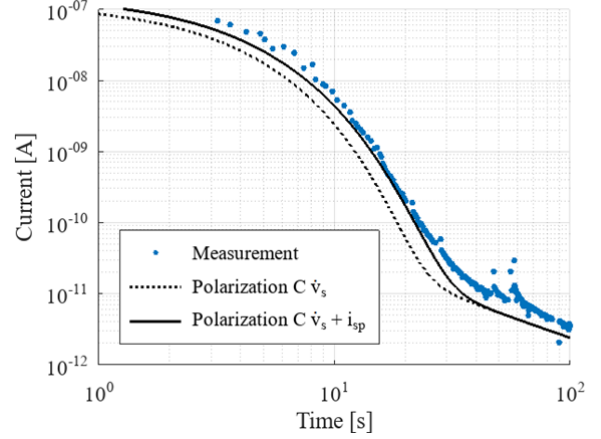


Fig. 16. Initial part of the depolarization transient in XLPE at 20 °C. The polarization processes seem to dominate in the first 20 s. One RC branch is introduced to improve the fitting. The current of the RC branch,  $i_{\text{sp}}$ , adds up to the current of the fast polarization processes,  $C \dot{v}_s$ .

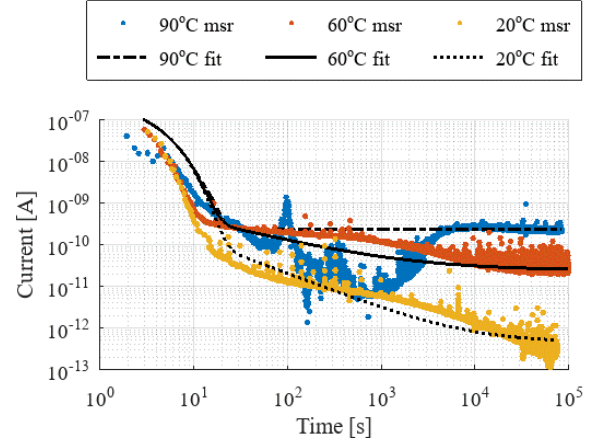


Fig. 17. Fitting polarization current measurements in XLPE at different temperatures. Measurements are labelled as “msr”, fittings are labelled as “fit”.

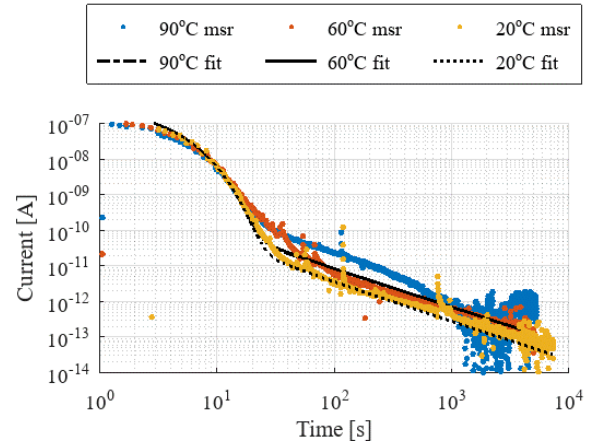


Fig. 18. Fitting depolarization current measurements in XLPE at different temperatures. Measurements are labelled as “msr”, fittings are labelled as “fit”.

The specimens were subject to an electric field of 30 kV/mm for  $10^4$  s at two temperatures levels, 30°C and 60°C for PP3, 20°C and 60°C for XLPE. Then the voltage was removed. The space charge considered here is the net one, obtained as the net balance between positive and negative charges. Charge  $\rho_s$  was then compared to the measured one,  $\rho_m$ . As an example, Fig. 19 shows the match between the space charge measured from XLPE at 20°C and its estimate from (24).

Table 5 compares  $\rho_s$  and  $\rho_m$  for PP3 and XLPE at the end of the polarization transient, i.e.,  $10^4$  s. The values do not perfectly match, but they are in the same order of magnitude. This suggests a correlation between space charge and the discrepancy in the fitting of the polarization currents.

**TABLE V**  
SPACE CHARGE STORED IN PP3 AND XLPE.

Samples	Space charge at $10^4$ s [ $\text{C}/\text{m}^3$ ]	
	Experimental, $\rho_m$ (mean on the latest 100 values)	Estimated, $\rho_s$
PP3 30 °C	0.44	0.62
PP3 60 °C	0.11	0.61
XLPE 20 °C	0.80	0.77
XLPE 60 °C	0.84	2.3

Space charge may also be involved in the initial stage of the depolarization transient. The charge here should be stored in the shallow traps, thus it is ready to leave the dielectric immediately after the beginning of the depolarization. Fig. 20 displays  $\rho_m$  obtained from the PEA measurements during the depolarization of PP3 at 60°C [28]. The first 20 s of the transient are affected by a non-negligible amount of fast-released (shallow-trapped) charge. This influences the behavior of the current in the initial part of the depolarization transient and hence the fitting.

Space charge may not be the only factor causing a discrepancy between model and experiments. As shown in Figs. 10, 12, 15 and 17 within the first seconds of the polarization transient the fitting is not good. The generator intrinsic transient, parasitic capacitances in the measurement system and a delay between the moment in which the voltage is applied to the sample and the one in which the measurement system starts the acquisition may have a non-negligible effect.

All these factors render the fitting of the initial polarization and depolarization transients a challenge. As an example, let us consider PP3 at 60 °C, that was shown in Figs. 14 and 15. The initial depolarization transient was properly fitted, but not the polarization transient. If we slightly modify the model for the generator during polarization by introducing a time-shift,  $t_s$ ,

$$v_s(t) = V \left( 1 - e^{-\frac{t-t_s}{\tau_g}} \right), \quad (25)$$

and we let  $t_s$  be -12 s, the fitting of the polarization curve becomes the one of Fig. 21. The fitting of the depolarization does not change with respect to Fig. 14. Compared to Fig. 15 the fitting in Fig. 21 is much better, but it carries the cost of a

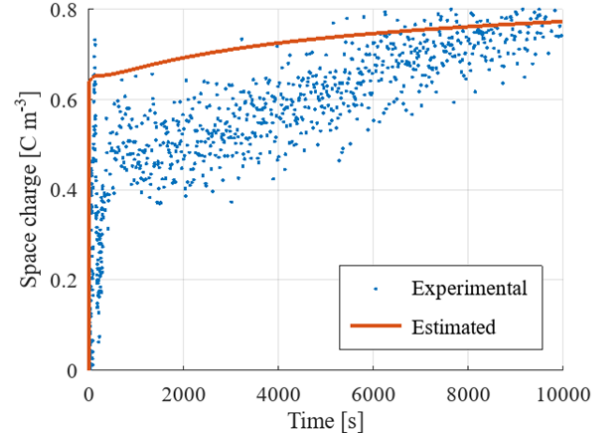


**Fig. 19.** Comparison of pace charges  $\rho_s$  (estimated) and  $\rho_m$  (experimental). XLPE at 20°C, during polarization.

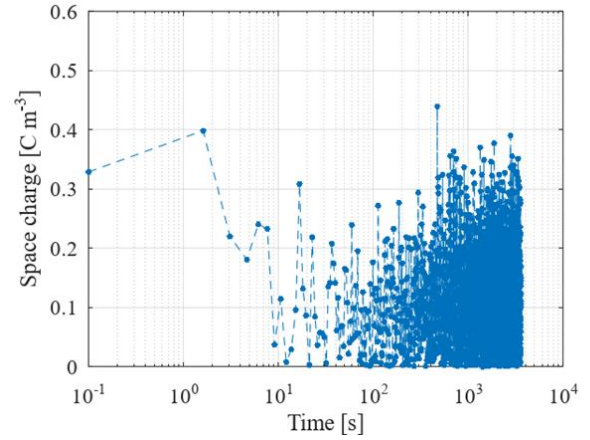


**Fig. 20.** Space charge transient measured in PP3 at 60°C during depolarization.

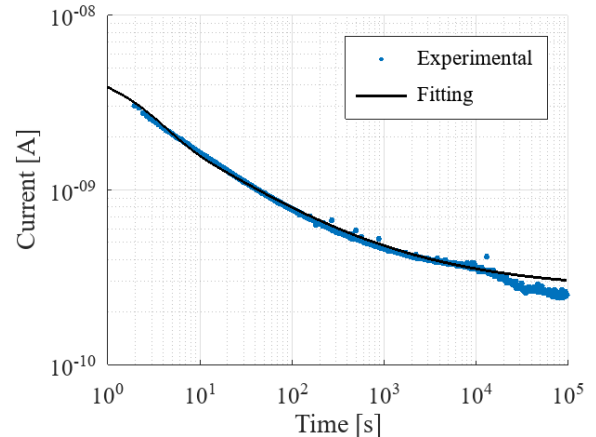


**Fig. 21.** Fitting of the polarization current in PP3 at 60°C after introducing the time shift  $t_s$ .

new parameter,  $t_s$ , that is due to the previously mentioned disturbing factors. It is important to observe that the introduction of this new parameter did not require to modify those associated with the shallow and the deep traps, that were

listed in Table 3. This means that even if many disturbances occur to the measurement in the first tens of seconds, the long-term transient is insensitive to them, thus the fitting of shallow and deep traps behavior is robust. Different experimental setups from the one used in this paper may attenuate some of the disturbing factors in the initial stage of the transients, allowing a better fitting of the model parameters over the whole testing time.

## VII. CONCLUSION

This paper proposes a circuital model to describe the PDC measured in polymeric materials. The model is valid under relatively low electric fields. The total number of parameters ranges from 7 to 9, depending on the type of available experimental results. The comparison between fittings and experiments shows that the model is qualitatively and quantitatively viable **in most situations**.

The discrepancy between model and experiments found on the medium-long term can be attributed to the dynamic of deep-trapped space charge. The fitting of the early seconds of the polarization and depolarization transients is challenging, as some disturbing factors (shallow-trap space charge release, testing procedure and equipment) may influence the behavior of the current. An experimental setup that attenuates some of the disturbances may allow a more robust fitting.

In conclusion, the presented model seems to provide an acceptable description of the polarization and depolarization currents in polymeric materials. The introduction of a parallel branch in the equivalent circuit of Fig. 1 to consider the dynamics of the deep traps can be interpreted as a generalization of the well-known extended Debye model.

## REFERENCES

- [1] G. C. Montanari, P. Morshuis, P. Seri and R. Ghosh, "Ageing and reliability of electrical insulation: the risk of hybrid AC/DC grids," *High Volt.*, vol. 5, no. 5, pp. 620–627, 2020.
- [2] H. Naderiallaf, P. Seri and G. C. Montanari, "Effect of voltage slew rate on partial discharge phenomenology during voltage transient in HVDC insulation: the case of polymeric cables," in *IEEE Transactions on Dielectrics and Electrical Insulation*, vol. 29, no. 1, pp. 215–222, Feb. 2022.
- [3] P. H. F. Morshuis and J. J. Smit, "Partial discharges at DC voltage: their mechanism, detection and analysis," in *IEEE Transactions on Dielectrics and Electrical Insulation*, vol. 12, no. 2, pp. 328–340, April 2005.
- [4] "IEEE Recommended Practice for Testing Insulation Resistance of Electric Machinery," in *IEEE Std 43-2013 (Revision of IEEE Std 43-2000)*, vol., no., pp. 1–37, 6 March 2014.
- [5] G. Teyssedre and C. Laurent, "Charge transport modelling in insulating polymers: from molecular to macroscopic scale," *IEEE Trans. Dielectr. Electr. Insul.*, vol. 12, no. 5, pp. 857–875, 2005.
- [6] G. Teyssedre, F. Zheng, L. Boudou and C. Laurent, "Charge trap spectroscopy in polymer dielectrics: a critical review," *J. Phys. D: Appl. Phys.*, vol. 54, 2021, Art. no. 263001.
- [7] T. Mizutani, K. Kaneko and M. Ieda, "Anomalous discharging currents due to space charge," *Jpn. J. Appl. Phys.*, vol. 20, no. 8, pp. 1443–1448, 1981.
- [8] S. Le Roy, G. Teyssedre, C. Laurent, L. A. Dissado and G. C. Montanari, "Relative importance of trapping and extraction in the simulation of space charge distribution in polymeric insulators under DC potentials," 2007 *IEEE International Conference on Solid Dielectrics*, pp. 494–497, 2007.
- [9] S. Le Roy, G. Teyssedre, C. Laurent, G. C. Montanari and F. Palmieri, "Description of charge transport in polyethylene using a fluid model with a constant mobility: fitting model and experiments," *J. Phys. D: Appl. Phys.*, vol. 39, pp. 1427–1436, 2006.
- [10] F. Baudoin, S. Le Roy, G. Teyssedre and C. Laurent, "Bipolar charge transport model with trapping and recombination: an analysis of the current versus applied electric field characteristic in steady state conditions," *J. Phys. D: Appl. Phys.*, vol. 41, 2008, Art. no. 025306.
- [11] Y. Zheng, H. Huang, X. Zhong and Y. V. Serdyuk, "Simulation of charge transport in polypropylene-based nano-composites," *J. Phys. D: Appl. Phys.*, vol. 54, 2021, Art. no. 235501.
- [12] J. Xue, Z. Zhang, M. Zhu, Y. Zhao and L. Ding, "Charge transport behavior in XLPE-insulated cables under DC and thermal gradient coupling field considering the effects of non-uniform conductivity," *J. Phys. D: Appl. Phys.*, vol. 54, 2021, Art. no. 485501.
- [13] P. C. Africa, C. de Falco, F. Maddalena, M. Caironi and D. Natali, "Simultaneous extraction of density of states width, carrier mobility and injection barriers in organic semiconductors," *Sci. Rep.*, vol. 7, 2017, Art. no. 3803.
- [14] P. Cambareri, C. de Falco, L. Di Rienzo, P. Seri and G. C. Montanari, "Charging and discharging current measurements and impact of polarization dynamics on electric field modeling in HVDC paper-insulated cables," *IEEE Access*, vol. 9, pp. 45155–45162, 2021.
- [15] H. J. Wintle, "Charge motion in technical insulators: facts, fancies and simulations," 2003 *Annual Report Conference on Electrical Insulation and Dielectric Phenomena.*, pp. 1–15, 2003.
- [16] X. He, P. Seri, I. Rytöluoto, R. Anyszka, M. Niittymäki, A. Mahtabani, H. Naderiallaf, E. Saarimäki, K. Lahti, M. Paajanen, W. Dierkes and A. Blume, "Influence of polar and unpolar silica functionalization on the dielectric properties of PP/POE nanocomposites," 2020 *IEEE 3rd International Conference on Dielectrics.*, pp. 229–232, 2020.
- [17] G. Mazzanti, G. C. Montanari and J. M. Alison, "A space-charge based method for the estimation of apparent mobility and trap depth as markers for insulation degradation – Theoretical basis and experimental validation," *IEEE Trans. Dielectr. Electr. Insul.*, vol. 10, no. 2, pp. 187–197, 2003.
- [18] A. K. Jonscher, *Dielectric Relaxation in Solids*, London: Chelsea Dielectrics Press, 1983.
- [19] M. Tavakoli, J. Hirsch, "Absorption current and depolarization measurements on polypropylene film," *J. Phys. D: Appl. Phys.*, vol. 21, pp. 454–462, 1988.
- [20] J. G. Simmons and M. C. Tam, "Theory of isothermal currents and the direct determination of trap parameters in semiconductors and insulators containing arbitrary trap distributions," *Phys. Rev. B*, vol. 7, no. 8, pp. 3706–3713, 1973.
- [21] Y. Zhang, J. Lewiner, C. Alquié and N. Hampton, "Evidence of strong correlation between space-charge buildup and breakdown in cable insulation," *IEEE Trans. Dielectr. Electr. Insul.*, vol. 3, no. 6, 778–783, 1996.
- [22] G. C. Montanari, "Bringing an insulation to failure: the role of space charge," *IEEE Trans. Dielectr. Electr. Insul.*, vol. 18, no. 2, pp. 339–364, 2011.
- [23] H. Yuan, Y. Zhou, Y. Zhu, S. Hu, C. Yuan, W. Song, Q. Shao, Q. Zhang, J. Hu, Q. Li and J. He, "Origins and effects on deep traps in functional group grafted polymeric dielectric materials," *J. Phys. D: Appl. Phys.*, vol. 53, 2020, Art. no. 475301.
- [24] P. Cambareri, C. de Falco, L. Di Rienzo, P. Seri and G. C. Montanari, "Simulation and modelling of transient electric fields in HVDC insulation systems based on polarization current measurements," *Energies*, vol. 14, no. 24, 2021, Art. no. 8323.
- [25] P. K. Watson, "The transport and trapping of electrons in polymers," *IEEE Trans. Dielectr. Electr. Insul.*, vol. 2, no. 5, 915–924, 1995.
- [26] E. Occhini, M. Maschio, "Electrical characteristics of oil-impregnated paper as insulation for HV DC cables," *IEEE Trans. Power Appar. Syst.*, vol. PAS-86, no. 3, pp. 312–326, 1967.
- [27] X. Cheng, G. Ye, H. Sun, T. Li and C. Sun, "Analysis of low-frequency dielectric loss of XLPE cable insulation based on extended Debye model," *AIP Adv.*, vol. 11, 2021, Art. no. 085103.
- [28] G. C. Montanari, P. Seri, M. Ritamäki, K. Lahti, I. Rytöluoto and M. Paajanen, "Performance of nanoparticles in the electrical behavior of DC capacitor films," 12th *International Conference on the Properties and Applications of Dielectric Materials (ICPADM)*, pp. 41–44, 2018.